

De Novo Inference of Systems-Level Mechanistic Models of Development from Live-Imaging-Based Phenotype Analysis

Zhuo Du,¹ Anthony Santella,¹ Fei He,¹ Michael Tiongson,¹ and Zhirong Bao^{1,*}

¹Developmental Biology Program, Sloan-Kettering Institute, New York, NY 10065, USA

*Correspondence: baoz@mskcc.org

<http://dx.doi.org/10.1016/j.cell.2013.11.046>

SUMMARY

Elucidation of complex phenotypes for mechanistic insights presents a significant challenge in systems biology. We report a strategy to automatically infer mechanistic models of cell fate differentiation based on live-imaging data. We use cell lineage tracing and combinations of tissue-specific marker expression to assay progenitor cell fate and detect fate changes upon genetic perturbation. Based on the cellular phenotypes, we further construct a model for how fate differentiation progresses in progenitor cells and predict cell-specific gene modules and cell-to-cell signaling events that regulate the series of fate choices. We validate our approach in *C. elegans* embryogenesis by perturbing 20 genes in over 300 embryos. The result not only recapitulates current knowledge but also provides insights into gene function and regulated fate choice, including an unexpected self-renewal. Our study provides a powerful approach for automated and quantitative interpretation of complex *in vivo* information.

INTRODUCTION

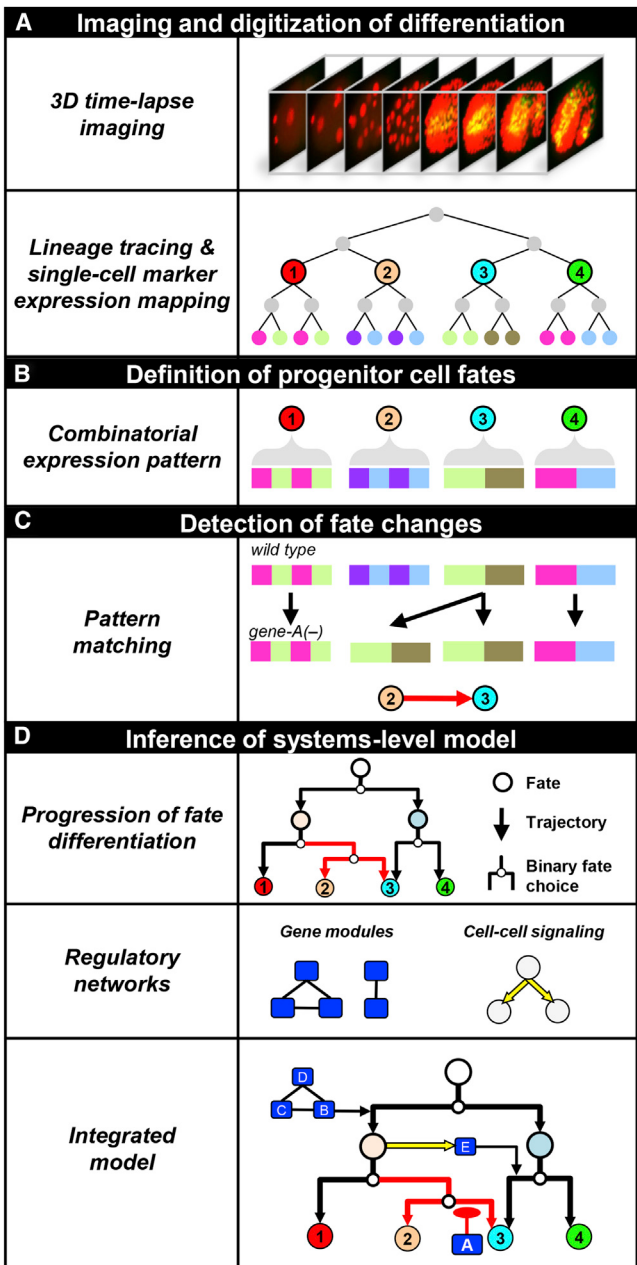
A desired framework for systematic understanding of biological processes would include regulatory networks from molecules to cellular behavior and then from cellular behavior to organismal function. Recent progress in 3D time-lapse imaging has provided an unprecedented opportunity to dissect complex *in vivo* phenotypes and achieve systems-level understanding of development (Megason and Fraser, 2007). In particular, development of diverse organisms can be imaged with single-cell resolution over an extended period of time (Busch et al., 2012; Keller, 2013). However, the biological complexity of development combined with the sheer amount of data from live imaging presents a significant challenge on how to extract useful phenotypic information and how to translate the information into mechanistic understanding.

C. elegans has proven to be an effective model for systems biology, especially for inferring gene networks based on *in vivo* phenotypes (Green et al., 2011; Gunsalus et al., 2005; Lehner

et al., 2006; Liu et al., 2009; Murray et al., 2012). In particular, developmental phenotypes during *C. elegans* embryogenesis can be systematically dissected on a cell-by-cell basis. *C. elegans* embryogenesis follows an invariant cell lineage to generate 558 differentiated cells (Sulston et al., 1983). The stereotypical cellular behaviors in proliferation, differentiation, and morphogenesis further simplify systematic single-cell phenotype analysis (Bao et al., 2008; Giurumescu et al., 2012; Hench et al., 2009; Moore et al., 2013; Schnabel et al., 1997; Sönnichsen et al., 2005). Highly automated cell lineage tracing has been developed based on 3D time-lapse imaging using fluorescently labeled histones to track cells (Bao et al., 2006; Mace et al., 2013). This automation opened a door to process developmental information from large image data sets.

In this study, we present an approach to infer systems-level mechanistic models of development de novo from live-imaging data based on automated phenotype analysis. Our study is focused on the regulation of cell fate differentiation. The fate of a progenitor cell is manifested as the distinct set of specialized cell types that it gives rise to. Following this concept, our approach uses cell lineage tracing and combinations of cell-type-specific marker expression to assay progenitor cell fate. It then uses automated reasoning to detect fate changes in individual progenitor cells upon genetic perturbation. In particular, it identifies homeotic transformations and infers the primary site of the fate phenotype. Based on the cellular phenotypes, it further constructs a directed graph as a model for how fate differentiation progresses in progenitor cells and predicts gene modules and cell-to-cell signaling events that regulate the series of fate choices. The automated reasoning and interpretation of phenotypes are based on general logic without prior knowledge of gene function or the expectation of specific phenotypes.

We validated our approach in *C. elegans* embryogenesis by perturbing 20 widely conserved regulatory genes. We assayed cell fate differentiation in over 300 embryos in strains expressing reporter transgenes for five tissue types. Our analysis successfully recovered the known phenotypes and functions of the 20 genes. The systems-level model essentially recapitulates the current understanding of differentiation in the early embryo. More importantly, the analysis identified 14 new phenotypes caused by inactivation of seven of the genes and six new types of homeotic transformations that reveal previously unknown binary fate choices in development. We further validated one of the insights, namely the turnover of a lineage specifier as a

**Figure 1. Strategy Overview**

- (A) Development was recorded by 3D time-lapse imaging. Differentiation was digitized by cell lineage tracing and determining single-cell expression status of tissue markers. See also [Movie S1](#).
- (B) Fate of progenitor cells (numbered circles) was defined retrospectively by assaying the combinatorial expression pattern (CEP) of tissue markers in resulting terminal cells.
- (C) Systematic comparison of CEPs between progenitor cells in wild-type and perturbed embryos detects fate changes. Homeotic transformations (red arrow) were identified.
- (D) Detected fate changes were used to infer a systems-level mechanistic model of how gene modules and cell-to-cell signaling events regulate fate choices as differentiation progresses.

binary switch between self-renewal and differentiation. These results demonstrate a powerful approach to analyze complex *in vivo* phenotypes using imaging to achieve a systems-level mechanistic understanding of development.

RESULTS

Design of Strategy

Our approach to infer mechanistic models of cell fate differentiation involves multiple layers of information processing. We first review the overall strategy of our approach here and then further describe the major components in the subsequent sections. As illustrated in [Figure 1](#), our approach consists of four major components:

Imaging and Digitization of Differentiation

We performed 3D time-lapse imaging of development and digitized the information on differentiation by systematic cell lineage tracing and tissue marker expression profiling at a single-cell resolution ([Figure 1A](#)).

Definition of Progenitor Cell Fate

We used a retrospective approach to define the fate of individual progenitor cells based on expression pattern of multiple tissue markers in terminal cells they give rise to ([Figure 1B](#)). The combinatorial expression pattern (CEP) can be thought of as a unique barcode to define the progenitor cell fate. To do so, we developed computational methods to synthesize CEPs from multiple markers, measure the similarity between CEPs, and classify the CEPs that capture the different progenitor cell fates in the wild-type.

Detection of Fate Changes

Upon genetic perturbations, we detected progenitor cell fate changes by comparing the CEPs of the progenitor cells between wild-type and perturbed embryos ([Figure 1C](#)). From the changes, we identified homeotic fate transformations where the fate of one progenitor cell is transformed to that of another. Our computational method incorporates automated reasoning to handle incomplete penetrance and pleiotropy and to infer the primary fate change.

Inference of Systems-Level Mechanistic Model of Differentiation

We combined cell lineage and fate assessment to infer how differentiation progresses in progenitor cells and used the detected fate transformations to infer regulated binary fate choices during the process ([Figure 1D](#)). In order to predict the gene modules and cell-cell signaling events that regulate the cascade of binary fate choices, we constructed gene-gene and cell-cell networks based on phenotypic similarities. Finally, all results were integrated into a mechanistic model revealing a molecular and cellular regulatory network controlling cell fate differentiation *in vivo*.

We validated our strategy in *C. elegans* embryogenesis by inferring the systems-level mechanistic model underlying the specification of 13 early progenitor cells that have been classically defined as founder cells. Each of these founder cells exhibits a distinct fate and gives rise to a distinct set of differentiated cell types ([Sulston et al., 1983](#)).

When developing the algorithms, we followed the general logic used in developmental genetics rather than *C. elegans*-specific

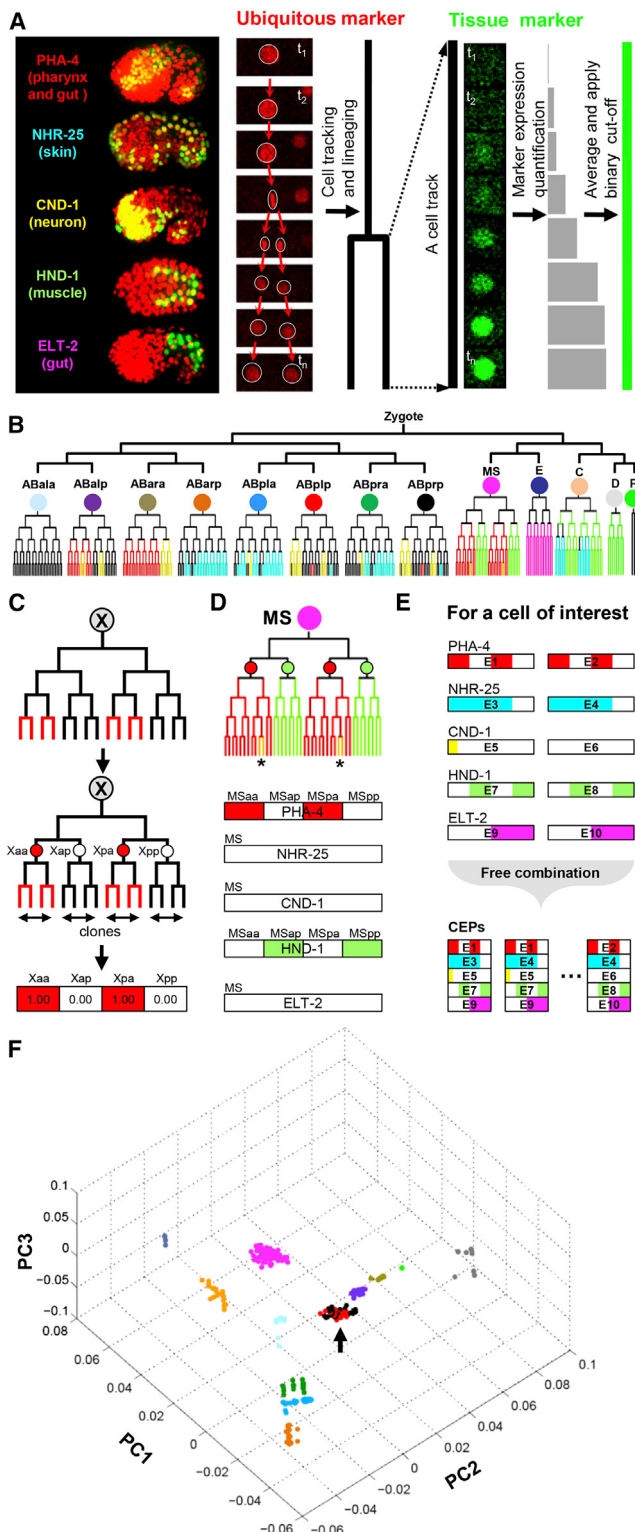


Figure 2. Experimental Definition of Progenitor Cell Fates

(A) Digitization of differentiation. Left: markers for the five major tissues. Middle: a ubiquitously expressed histone marker (red) was used for de novo construction of cell lineage. Right: expression level of tissue marker (green) was measured at every time point and averaged over a cell's lifetime

rules. In the following sections, we describe the specific design of each component as well as the key technical and biological considerations. Due to space limitations, more detailed information is provided in [Extended Experimental Procedures](#). When appropriate, we describe the performance and validation of our methods.

Imaging and Digitization of Differentiation

To profile the differentiation of embryonic cells, we performed 3D time-lapse imaging to record embryogenesis and used automated image analysis to track cells and assay tissue marker expression ([Bao et al., 2006; Murray et al., 2008, 2012; Santella et al., 2010](#)). Specifically, we used a ubiquitously expressed histone-fluorescent protein fusion to label all cells, which allowed us to track every cell and reconstruct the cell lineage. An additional fluorescent protein fused to a tissue-specific gene allowed us to determine the cell type ([Figure 2A](#)). Overall, we used five strains, each carrying a ubiquitously expressed marker and a tissue-specific marker, to systematically profile the differentiation of the major tissue types of *C. elegans* ([Figure 2A](#); [Table S1](#) available online).

We imaged embryogenesis at a fine temporal resolution (75 s) for the first 7 hr of development ([Movie S1](#)). We digitized the process by tracing the entire cell lineage and measuring marker expression through the first nine out of a total of ten rounds of cell division. By this stage, the embryo contains about 350 cells and has completed gastrulation and major tissue/organ patterning, providing sufficient information about differentiation ([Sulston et al., 1983](#)). Each digitized embryo contains quantitative data on the position and marker expression level of every cell at every time point. For this study, we further processed the information to a binary call on whether a cell expresses a tissue marker or not ([Figures 2A, S1A and S1B](#)).

to determine the tissue type of individual terminal cells. See also [Figures S1A and S1B](#).

(B) A consensus cell lineage and marker expression patterns. The 13 founder cells of interest are indicated using colored circles and cell names. Colors in lineage tree indicate expressing cells for each marker. Black branches represent nonexpressing cells. See also [Figure S1C](#).

(C) Quantitative description of expression patterns via clonal expression analysis. For a given marker within the sublineage of a given founder cell (X), maximal clones with uniform expression and significant size (horizontal arrows) were identified. The lineal ID of the progenitor of each expressing and nonexpressing clones (red and white dots) and the frequency of expressing cells within each clone were used to describe the expression pattern of the marker. See also [Figures S1D–S1F](#).

(D) CEP of five markers captures fate of a corresponding progenitor cell. Figure shows the CEP for the MS cell. Note that the yellow branches (stars) show consistent expression of the CND-1 marker, but no expressing clones were defined (CND-1 in bottom), because of the nonsignificant clone size.

(E) Free combination of single-marker expression patterns to synthesize CEPs. Each barcode represents a single-marker expression pattern for a cell of interest. CEP was synthesized using a free-combination strategy and for each CEP one expression pattern per marker was used.

(F) Classification of CEPs. 3D scatter plot shows the distribution of wild-type CEPs in an abstract space. The three axes are the first three principal components, which are abstract orthogonal dimensions suggested by a principal-component analysis (PCA) that show the highest variance among the samples (CEPs). CEPs belonging to different founder cells are in different color as in (B). Arrow indicates CEPs of ABplp and ABprp. See also [Figures S1G and S1H](#).

CEP-Based Assessment of Progenitor Cell Fate

A progenitor cell generates a specific set of cell types. For a given progenitor cell, we assayed its fate retrospectively using the CEP of tissue-specific markers in its sublineage (Figure 2B). We describe below three key aspects for using CEPs to systematically and objectively detect progenitor fates: (1) the set of tissue markers used, (2) the computational approach to define CEPs, and (3) methods to compare and classify the CEPs of different progenitor cell fates.

Selection of Markers

We used five well-characterized tissue-specific genes to generate the CEPs used to distinguish progenitor fates. These genes encode master transcription factors that drive the differentiation of the major tissue/cell types of *C. elegans*, namely *nhr-25* (skin), *cnd-1* (a subset of neurons), *pha-4* (pharynx and gut), *eit-2* (gut), and *hnd-1* (body wall muscle). We used available protein fusion fluorescent reporters for these genes, which are integrated into the genome. The expression pattern of these markers agrees well with the known function and endogenous expression of these genes in the literature. Details on these markers, including gene function, expression patterns, transgenic methods, and supporting literature, are provided in Table S1.

The major consideration in selecting a marker was its ability to distinguish the different founder cell lineages. An ideal marker would generate unique and easily distinguishable lineage patterns of expression for different progenitor cells, and a given set of markers should generate unique combinations of lineage patterns for each of the progenitor cells of interest (Figure 2B). Furthermore, the expression pattern should be reproducible so that the pattern can be reliably compared between embryos. The five markers used all showed high reproducibility ($r > 0.9$, $n = 10$ for each marker; Figure S1C). They were also sufficient to generate distinguishable combinatorial patterns as readouts of early progenitor cell fates (see below). In short, for a useful marker, the uniqueness and reproducibility of lineage expression pattern are more important than the precise tissue details of its expression pattern. Our use of five markers was a practical decision to balance workload and the risk of erroneous fate calls. Additional discussions regarding marker choice are provided in the Extended Experimental Procedures (General Considerations).

Computational Approach to Define CEPs

Our computational definition of CEPs included two steps: (1) define the expression pattern of a single marker in a sublineage and (2) combine the patterns of multiple markers into a CEP.

To define the expression pattern of a single marker in a given sublineage, we described the pattern as a set of clonal expression sites (Figure 2C). A clonal expression site is a maximal clone (horizontal arrows in Figure 2C) with uniform expression (fraction of expressing cells within the clone > 0.85) and significant size (binomial test, $p < 0.01$; Extended Experimental Procedures). The expression pattern was then described as a list of the expressing and the complementary nonexpressing clones. Each clone was described by two factors: the lineal identity of the founder cell of the clone (red and white dots and cell names in Figure 2C) and the fraction of expressing cells within the clone (numbers 1.00 and 0.00 in Figure 2C). Biologically, the clonal sites reflect the underlying differentiation program within a given

sublineage. In particular, the lineal identity of the clonal sites reflects the invariable developmental programs in the lineage. Technically, the use of clonal sites provides robustness to the subsequent computational analyses in terms of variations of marker expression and lineage errors (see Extended Experimental Procedures, General Considerations).

To combine the expression pattern of multiple markers into a CEP, we simply used a list of each marker's pattern (Figure 2D). The number of markers that can be assayed in a single specimen through live imaging is limited due to technical considerations. Therefore, we developed computational methods to combine the expression of different markers from multiple embryos. A key step in doing so was to identify the equivalent cells across embryos. The general approach requires anatomy-based alignment between specimens (e.g., corresponding tissue layers after spatial alignment). However, because of the invariant cell lineage in *C. elegans* and the stereotypical orientation of each mitosis (Sulston et al., 1983), the lineal name of a cell provides the equivalent information to its anatomical position. Therefore, in our approach, cells with the same lineal name in different embryos were taken as equivalent cells.

We imaged multiple embryos for each tissue-specific marker. To synthesize the CEP for a given cell, we exhausted all combinations of the defined single-marker expression patterns for that cell, with each combination containing one defined pattern per marker (Figure 2E). For example, if two embryos were imaged for each of the five markers, this would yield $2^5 = 32$ instances of CEP for a given cell. With a naive approach to enumerate all combinations, the computational load will increase exponentially with the number of markers used. To reduce the computational task, we developed an algorithm where the amount of computation increases linearly with the number of markers (see Extended Experimental Procedures). Implications of this free-combination approach are addressed below in "Detection of Fate Changes."

Methods to Compare and Classify CEPs

In order to use CEPs to assay progenitor cell fate, we first developed methods to quantify pairwise similarity between CEPs. We then defined the distinct classes of CEPs among the 13 founder cells in the wild-type embryos. Combining these two pieces allowed us to assay the fate of a progenitor cell by comparing its CEP to the wild-type CEP classes.

To determine how similar two CEPs are, we calculated an abstract distance between the two. Specifically, we enumerated each clonal expression site of each marker, calculated the difference in the fraction of expressing cells at each site, and summed the differences to compute the distance (Figure S1E; Extended Experimental Procedures). Using this quantitative measure of similarity, we examined the CEPs of the 13 founder cells based on the five markers in 50 wild-type embryos (ten embryos for each marker). We found that the CEPs fell in 12 distinct classes. The intraclass distances were significantly less than the inter-class distances (Figures 2F and S1H; t test, two tailed, $p < 0.001$). The fates of the ABplp and ABprp cells were indistinguishable (arrow in Figure 2F). The differences between the two are known to be subtle, which involve a handful of terminal cells at sub-tissue-type level (Sulston et al., 1983). Hence, with the five markers, our CEP-based approach can distinguish 12 unique progenitor cell fates.

The above analysis also allowed us to define the consensus and variance for each of the 12 classes of wild-type CEPs (Figure S1I), which were in turn used as references to classify the CEPs observed in progenitor cells in mutants/RNAi. An observed CEP is considered a match for one of the 12 classes if the distance to the reference is statistically indistinguishable from the corresponding intraclass distance (t test, $p > 0.05$).

The above clonal-site-based description of expression pattern maximizes the use of information provided by an invariant lineage. To consider the more general cases where the sublineage of a founder cell could be variable, we also developed an alternative definition that describes the pattern as the fraction of terminal cells expressing a marker within the entire founder cell lineage (Figure S1D). This approach forgoes the lineage structure and the biological assumption of fate commitment in intermediate cells, making it broadly applicable to different developmental scenarios. CEPs defined by this alternative approach were sufficient to distinguish the 12 major progenitor cell fates (Figures S1G and S1H), demonstrating that the general strategy of CEP-based automated assessment of cell fate is not restricted to invariant cell lineages. As expected, this fraction-based approach was less robust in distinguishing CEPs with fine differences in marker expression patterns (circles in Figure S1G; see also Figures S1E and S1F for comparison). We therefore used the clonal-site-based definition in subsequent analyses.

Detection of Fate Changes

We used the 12 defined wild-type CEP classes to detect progenitor cell fate changes in perturbed embryos. In particular, we identified homeotic transformations among the detected changes. We developed computational methods for automated reasoning based on general logic of developmental genetics. These methods were designed to detect fate changes in the face of complication from incomplete penetrance and pleiotropy and to infer the primary fate changes from secondary phenotypes.

General Strategy

The 12 classes of wild-type CEPs were used as a reference to detect the occurrence of the 12 fates in the progenitor cells of perturbed embryos (Figure 3A). In addition to examining the 13 founder cells, we also examined their ancestor and daughter cells to assess potential premature and delayed differentiation phenotypes. Thus, we examined 51 progenitor cells in total (Figure S2A). Logical rules to reconcile the results when fate changes are detected in both a cell and its mother are defined in Extended Experimental Procedures.

Three outcomes of CEP detection are expected (Figure 3B): (1) the CEP of a progenitor matches its wild-type counterpart, suggesting no fate change; (2) the CEP of a progenitor matches a CEP that is normally associated with another progenitor, suggesting a homeotic transformation; and (3) the CEP of a progenitor matches none of the defined wild-type classes, suggesting that the progenitor cell adopts an undefined/uninterpretable fate. A typical example of (3) is global dysregulation of gene expression.

Incomplete Penetrance

When a phenotype is not fully penetrant, the same cell may exhibit different fates in different embryos (wild-type fate in some embryos and perturbed fate in others). As described above, we synthesized CEPs from multiple embryos by freely

combining across all embryos and markers. This free-combination approach has a distinct advantage in handling incomplete penetrance: the different fates are included in the set of synthesized CEPs as distinct CEPs instead of being averaged into a meaningless pattern. However, the free combination will also lead to artificial CEPs where expression patterns from different fates are mixed (Figure 3C).

We used two strategies to address these artifacts. First, we examined if a mixture of two wild-type classes of CEPs would generate an artificial CEP that matches a third fate following free combination. We simulated all pairwise mixtures ($12 \times 11/2 = 66$ pairs) and detected only one type of artificial match under our similarity measure and cutoffs, namely the CEP of ABala. This is because none of the five markers used is expressed in the ABala lineage and an all-blank CEP is expected to arise as an artifact given the restricted expression of the tissue-specific markers. In order to address this limitation, we developed methods to process the artificial ABala fate when it occurred (Extended Experimental Procedures). Second, we allowed multiple classes of CEPs to be detected for a given cell but only accepted undefined CEPs (undefined/uninterpretable fates) when no homeotic transformations were detected (Figure 3D). This rule allowed the detection of bona fide uninterpretable fates while avoiding the artificial combinations.

Pleiotropy

When a gene functions in many cells, the pleiotropic phenotype is naturally elucidated by our cell-by-cell analysis. When a gene has multiple functions in a cell, its disruption may produce different fate outcome in the cell across embryos in combination with incomplete penetrance. Needless to say, the methods above also apply here. It is worth noting that the methods above accept multiple distinct homeotic transformations for a cell, which cope with multiple gene functions (Figure 3D).

Primary Sites of Homeotic Transformation

Some of the homeotic transformations detected are expected to be secondary phenotypes derived from earlier changes in their ancestor cells. We developed methods to infer primary phenotypes from the detected changes so that the results would be more indicative of the regulatory mechanisms. We followed the parsimony principle to infer the primary site of transformation: when transformations were detected in both sister cells, we assumed that a transformation occurred in the mother cell, and we did so iteratively to find the earliest one (Figure 3E). Additional rules to infer primary sites and the new fate of a primary site are detailed in Extended Experimental Procedures and Figures S2B and S2C. It is worth noting that these inferred sites are primary site of homeotic transformation, but they could still be secondary phenotypes in terms of gene function.

In summary, our CEP-based phenotype analysis systematically detects and processes fate changes in individual progenitor cells during development. It reports primary sites of fate changes and classifies changes as homeotic transformations or fate dysregulation (Figure S2A).

Validation of Methods: De Novo Phenotype Analysis of Master Developmental Regulators

We applied the above approach to 20 genes that are well known as key regulators in diverse biological processes (Figure 4A). All 20

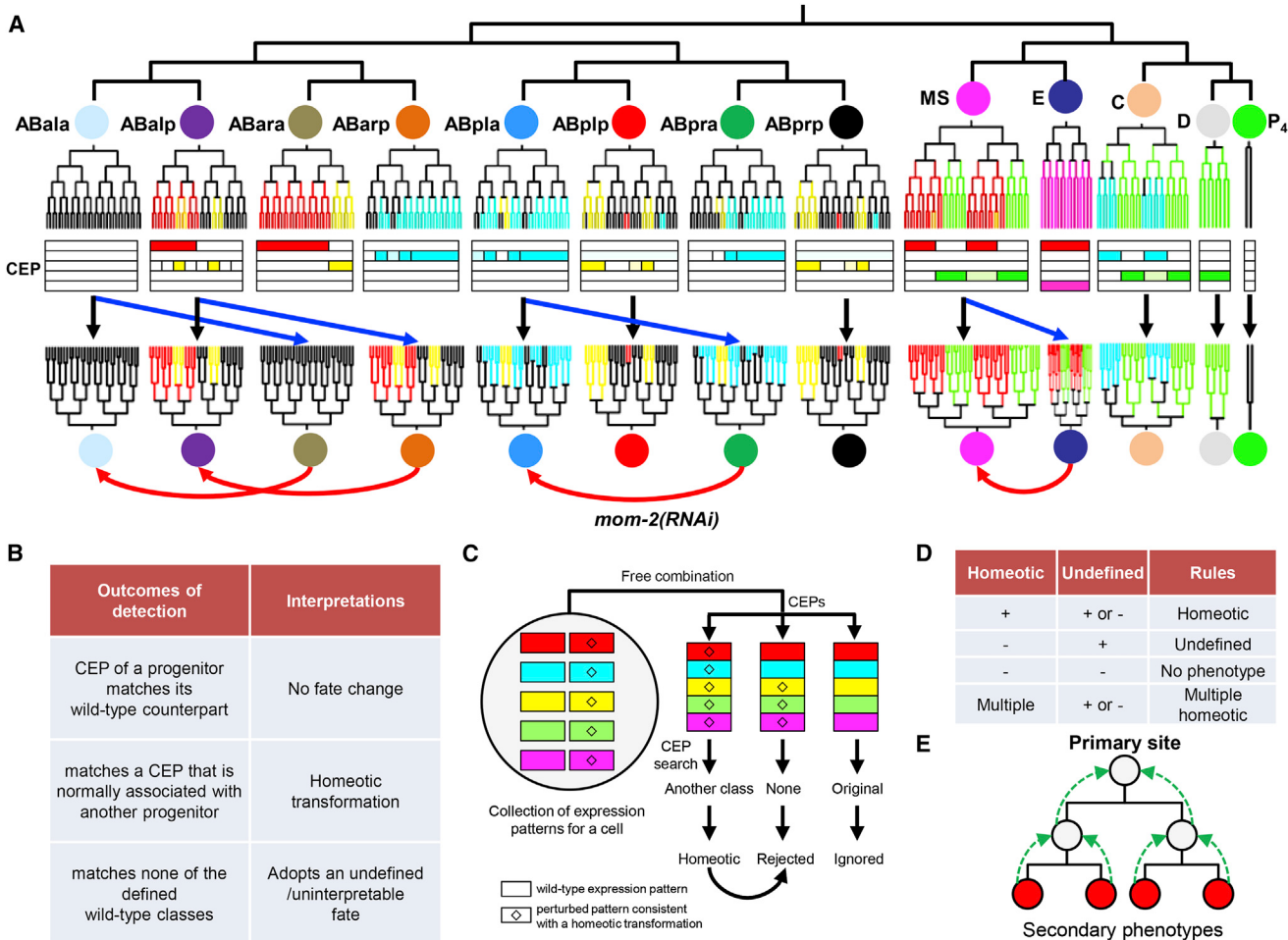


Figure 3. Detection of Cell Fate Changes

(A) Detection of fate changes by CEP match. Wild-type CEPs (top) were used to systematically detect the occurrence of the 12 founder fates in progenitor cells of perturbed embryos (bottom) based on quantitative comparison (arrows). MOM-2 is the *C. elegans* homolog of Wnt. Red arrows indicate detected homeotic transformations. See also Figure S2A.

(B) Three outcomes of CEP detection and their interpretations.

(C) Complications caused by incomplete penetrance. Free combination generates artificial CEPs in the presence of incomplete penetrance. Figure shows an example where a cell exhibits the wild-type fate and the corresponding single-marker expression patterns (left column) in some embryos and the transformed fate and expression patterns in others (right column). Each box represents a single-marker expression pattern and color represents type of marker. The artificial CEP would not match any defined wild-type CEP classes. It is rejected if another CEP is interpreted as a homeotic transformation (see B and D).

(D) Rules to process phenotype outcomes under incomplete penetrance. + and – indicate presence and absence, respectively. See the [Extended Experimental Procedures](#) for details.

(E) Parsimony to infer primary fate change. When transformations (red) are detected in both sister cells, we assume a change in the mother cell and do so iteratively to find the primary change. See also Figures S2B and S2C.

genes have been characterized to some extent in *C. elegans*, providing a solid and extensive benchmark to test our approach. We used RNAi to knock down each gene and analyzed two to six embryos for each of the five markers, totaling 260 embryos (Figures 4B–4D). Together with 50 wild-type embryos, our data set contains 310 embryos (Tables S2 and S3). Using the above methods, we detected 95 fate changes, including 23 deduced primary sites. Of these, 55 are detected as homeotic transformations, involving 17 pairs of progenitor cell fates (Figure 4E; Table S4).

We benchmarked the accuracy of these results in the following two ways. First, we examined the classification of the observed

CEPs. The new CEPs after the presumed homeotic transformations clustered tightly with the corresponding class in the wild-type (Figure 4F), suggesting that the detected transformations under our similarity measurements and cutoff are clean and valid. More specifically, our experimental data included single-marker expression patterns in 3,380 (13 × 260) founder cell sublineages (Figure 4G). Of these, 3,006 or 89% matched a wild-type counterpart. The remaining cases fell in three categories based on human evaluation. A total of 5.4% were deemed slight variations of the wild-type counterpart, which were rejected by our stringent cutoff. A total of 2.1% were deemed

partial transformations. The last category (3.5%) involved two situations: dysregulation of differentiation (such as in *hda-1*/HDAC) or complex functions in the sublineage that affect the expression pattern (such as *pop-1*/TCF). Second, we compared the 55 detected homeotic transformations to the literature. We correctly captured 22 out of 25 known phenotypes (Figure 4H; Table S4). The discrepancy came from three categories. The first was the absence of phenotypes, presumably due to the low penetrance of phenotypes in our RNAi treatments (e.g., *pal-1*/Caudal and *src-1*/FYNN). The second was due to complex function of a gene in the sublineage that affects the tissue marker expression pattern (e.g., *pop-1*/TCF), so that the result could not be matched to the expected CEPs. The third was insufficient merging of secondary sites into the known primary site of fate change. This affected only one situation in our data, namely, the transformation of ABp to its sister ABa upon the loss of first Notch induction (Schnabel and Priess, 1997). The complication arises because the progeny of the transformed ABp receive ectopic fate inductions subsequently, so that the tissue marker expression pattern does not perfectly match the ABa progeny pattern. For clarity, we manually corrected the case in the third category in Figure 4E. Both the second and third categories reflect our choice to match cell fate with caution and stringent cutoffs. Furthermore, of the 33 phenotypes that have not been reported before, 19 can be deduced from the literature (Figure 4H; Table S4), further validating the accuracy of our results.

Importantly, our results revealed 14 new phenotypes for 7 of the 20 genes (Table S4), including 6 new types of homeotic transformations. It is worth noting that many of these new phenotypes were detected based on the inactivation of highly pleiotropic genes, such as *gsk-3/gsk3β* and *skr-1/2/Skp1*. These results demonstrate that our methods are particularly powerful in elucidating pleiotropic effects that are composed of many specific phenotypes while refraining from overinterpreting global dysregulation. Furthermore, our methods also successfully handled the complex situation of a gene with nested multiple functions in a lineage, such as in the cases of *glp-1*/Notch in the ABp lineage or *skr-1/2/Skp1* in the C cell (Figure 4E). This is due to the incomplete penetrance of earlier functions in our RNAi treatments that allows the phenotypes of a later function to be observed and to the ability of our methods to synthesize CEPs from alternative phenotypes while rejecting artificial combinations of expression patterns.

In summary, our approach successfully recapitulates known gene functions in embryogenesis while also identifying new gene functions and types of homeotic transformations.

Validation of a New Phenotype: Protein Degradation Drives Transition of Cell Fate

A particularly interesting type of homeotic transformation occurred when a daughter cell adopts the fate normally associated with its mother cell, that is, self-renewal. RNAi depletion of *skr-1/2/skp1*, a component of the SCF E3 ubiquitin ligase component, caused such phenotypes in several blastomeres, including EMS, C, and P₃ (Figure 4E). These results raised the possibility that protein degradation controls the choice between self-renewal and differentiation and drives timely progression of cell fate.

To examine this possibility, we investigated the function of *skr-1/2* in one of the cases, namely, the endomesoderm differentiation in the EMS lineage. The endomesoderm is derived from a single blastomere at the four-cell stage named EMS. A sharp transition of fate occurs upon EMS division. The anterior daughter, named MS, differentiates into future mesoderm, whereas the posterior daughter, E, differentiates into the future endoderm (Figure 5A).

We first verified that in *skr-1/2(RNAi)* the anterior daughter, MS, reiterated the EMS fate. In addition to the general tissue fate patterning that led to the automated prediction (Figure 5B), we found extensive evidence that MS generated the precise EMS lineage, including using additional transgenic reporters (Table S5), single-cell behaviors (programmed cell death, spindle orientation, gastrulation), cell proliferation, and overall tissue morphogenesis (Figures S3A–S3D). Second, we found in *skr-1/2(RNAi)* the EMS blastomere behaved as in the wild-type: it showed molecular and cellular behaviors that are specific to the wild-type EMS blastomere (Figures 5C and 5D). Collectively, these results suggest a reiteration instead of delayed specification of EMS fate or a dramatic fate change of early blastomeres. Similarly, we found that loss of function of another component of SCF (the Culin protein CUL-1/CUL1, n = 9) and a subunit of the 26S proteasome complex (RPN-8/PSMD7, n = 2), phenocopied *skr-1/2(RNAi)* (Figures S3E and S3F). These results suggest that *skr-1/2* functions through the SCF E3 ligase complex-mediated protein degradation to promote the transition of cell fate from EMS to its anterior daughter.

We found that *skr-1/2* promoted EMS fate transition by restricting the temporal expression of SKN-1/Nrf1/2, a conserved bZip transcription factor that specifies the EMS fate (Bowerman et al., 1992). During normal development, SKN-1 shows transient expression in the EMS blastomere but rapidly diminishes upon EMS division so that no SKN-1 is detectable in later-stage EMS daughter cells (Bowerman et al., 1993; Page et al., 2007). We found that *skr-1/2* was required for timely degradation of SKN-1 during EMS-to-MS transition. We used a SKN-1::GFP reporter to monitor SKN-1 expression (Page et al., 2007). In *skr-1/2(RNAi)*, the initial level in the EMS blastomere was comparable to the wild-type. However, the reduction of protein level over time was significantly dampened and SKN-1 persisted for an additional cell cycle (Figure 5E). Importantly, we found that delayed degradation of SKN-1 caused EMS self-renewal. We overexpressed SKN-1::GFP under a heat-shock promoter. After heat shock, a high level of SKN-1::GFP was induced and sustained for approximately one additional cell cycle in the EMS lineage (Figure 5F). Concomitantly, we detected reiteration of the EMS fate (n = 15). Quantitative analysis of cell fate showed that as in *skr-1/2(RNAi)*, in SKN-1 overexpression the CEPs of the MS cell was indistinguishable from that of wild-type EMS fate (Figure 5G; CEP distance = 0.05 and = 0.03, p = 0.6 and 0.8, respectively) but was significantly different from that of wild-type MS fate (CEP distance = 1.49 and 1.48, p = 0 for both cases). More significantly, two rounds of EMS reiteration were induced when SKN-1::GFP was sustained for two additional cell cycles (Figure S3G; n = 7). Taken together, our results suggest that SCF controls self-renewal by promoting the turnover of SKN-1.

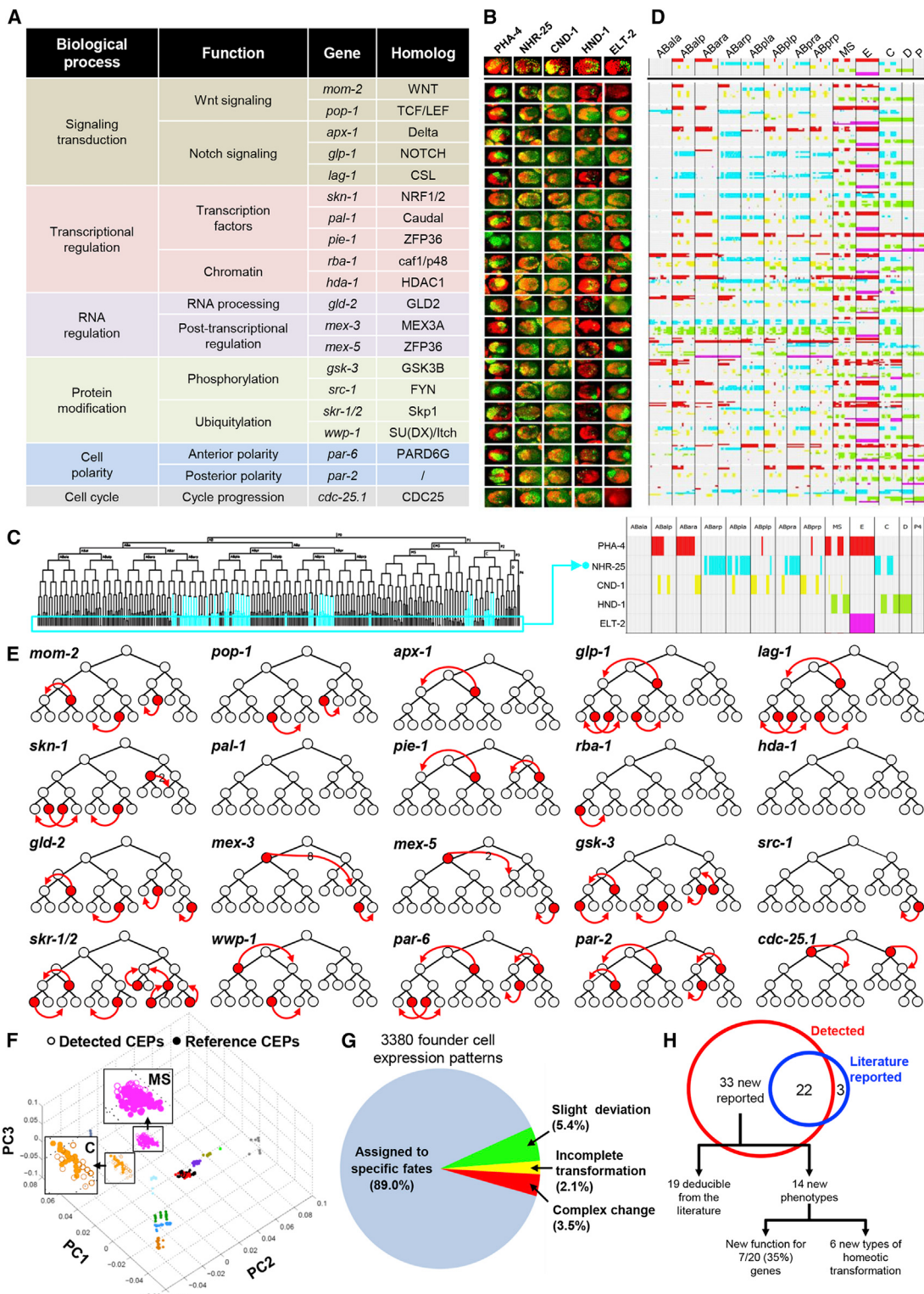


Figure 4. De Novo Phenotype Analysis of Master Developmental Regulators

(A) List of the 20 genes examined.

(B) Representative micrographs (3D projections) showing the terminal phenotypes of RNAi. Top row shows the wild-type.

(C) Heatmap display of expression patterns. Marker expression in terminal cells (cyan box in left) was used as a summary heatmap for display. Cells are ordered based on the lineage, with founder cell names listed on top. Different tissue markers are in different colors as in Figure 2A.

(legend continued on next page)

In all, the above results validated the automatically detected *skr-1/2(RNAi)* phenotype as a fate reiteration/self-renewal of EMS and further dissected the underlying mechanism where protein degradation of a master transcription factor controls progression of differentiation (Figure 5H). The analysis of cell fate at single-cell resolution pinpoints the phenotype to a failure of fate transition between a mother cell and its daughters, ruling out alternative explanations that gross terminal phenotype assays could not eliminate, such as impaired execution of downstream differentiation or mitotic exit. These results show that turnover of a lineage specifier functions as a binary switch between self-renewal and differentiation.

Systems-Level Model of Differentiation

Finally, we analyzed the detected cell fate phenotypes to infer a systems-level mechanistic model of differentiation. The model consists of three components: (1) a directed graph representing how fate differentiation progresses over development along with the fate choices during the process, (2) cell-specific gene modules, and (3) cell-cell signaling events that regulate fate choices.

Fate Progression and Fate Choices

We used a directed graph to represent the progression of cell fate (Figures 6A and 6B). In such a graph, nodes represent the progenitor cell fates, arrows represent the trajectories of fate progression, and bifurcations represent fate choices. Differentiation during normal development can be inferred from the wild-type cell lineage, which yields trajectories of fate progression bifurcating from the mother to two daughter-cell fates (Figure 6A, top). Homeotic transformations reveal additional binary fate choices. Each transformation between non-sister-cell fates reveals such a fate choice that is not evident from normal development. In these cases, we added a new arrow bifurcating from the mother to two fates (Figure 6A, bottom). For transformations between sister-cell fates, the binary fate choice is already captured by the bifurcations constructed from the wild-type (Figure 6A, middle).

By integrating all detected homeotic transformations, the resulting graph provides a model of fate progression during development (Figure 6B). The model includes 24 progenitor fates observed in the wild-type (12 founder cell fates and 12 ancestor cell fates) and three non-wild-type ancestor fates (see Extended Experimental Procedures for definition and Figure S2C). It also represents 26 binary fate choices (points in Figure 6B). Six of these are new fate choices revealed by this study (red stars in Figure 6B). Fate choices between nonsister fates reflect non-deterministic differentiation in *C. elegans* (Schnabel and Priess, 1997) as well as multipotent and reprogrammable fates in the early blastomeres.

Gene Modules and Cell-Cell Signaling

Fate changes implicate the perturbed genes as regulators of differentiation. In total, we identified 55 homeotic transformations

caused by loss of the 20 genes (Figure 6C). The cellular resolution of phenotypes allowed us to further analyze the regulatory mechanisms in terms of gene modules and cell-to-cell signaling events that regulate fate choices. We did so by constructing gene-gene and cell-cell networks.

We first constructed a gene network by measuring phenotypic similarity between genes. We measured phenotypic similarity by calculating the pointwise mutual information between genes (see Extended Experimental Procedures for details). Because of the directionality of homeotic transformations (Figure 6D), our analysis was able to link not only genes with the same regulatory function but also those with opposite functions (red and blue edges in Figure 6E, respectively). Of the reported edges in the network (Figure 6E), those with two or more shared phenotypes are highlighted with thick lines. The predicted gene network successfully captures the three known molecular modules contained in the 20 genes, namely, the Notch pathway, the Wnt pathway, and the PAR polarity pathway (dashed circles). All other thick edges are also consistent with the literature (Table S4), except those between *gld-2* and the Wnt pathway, which have not been reported before. *GLD-2* is an RNA-binding protein in the germline and the Wnt pathway components functioning in the early embryo are provided maternally. Therefore, we consider these thick edges a prediction that *gld-2* regulates the Wnt pathway, which remains to be tested experimentally.

Furthermore, the cellular-resolution phenotypes allowed us to construct a cell-cell network. The cell-cell network links cells that show correlated fate changes across perturbations (Figure 6F). We quantified the degree of correlation by calculating the pointwise mutual information between cells. We used this cell-cell network to predict cell-to-cell signaling events. This was based on the argument that if the fate of a signaling cell is perturbed, then the fate of the receiving cell should show correlated changes. An alternative reason for apparently correlated changes between cells is that the perturbed gene functions independently in the two cells. To minimize the inclusion of this alternative scenario, the cell-cell network was filtered by additional information such as cell position (i.e., potential cell contact) and independence of phenotypes in two cells within each individual embryo (Extended Experimental Procedures). The resulting network includes 12 cell pairs. These results capture all six known signaling events in the studied time window, namely, the four Notch signaling events (Schnabel and Priess, 1997) and two Wnt signaling events (Eisenmann, 2005). The predicted Notch and Wnt signaling events are confirmed by the phenotypes in the presumptive receiving cells caused by the genes in these pathways (green boxes in Figure 6F). Only three of the 12 pairs are potentially false-positive predictions where correlated fate changes reflect independent functions of genes in two cells. This cell-cell network analysis enriches for cell-to-cell

(D) Heatmap display of the five markers in the 260 RNAi-treated embryos in this study. Each row is an embryo as in (C) with the same color scheme. Top row shows the wild-type expression pattern. See also Table S3.

(E) Detected primary sites of homeotic transformations. Affected cells are in red and the arrows represent the type and direction of transformation.

(F) 3D scatterplot shows the distribution of CEPs that are classified as homeotic transformation (open circles) and the corresponding wild-type references (dots). The wild-type classes are organized as in Figure 2F. Two classes with the highest variability (associated with the MS and C fates) are shown in insets.

(G) Classification of founder cell CEPs in all RNAi-treated embryos.

(H) Summary of literature comparison. See also Table S4.

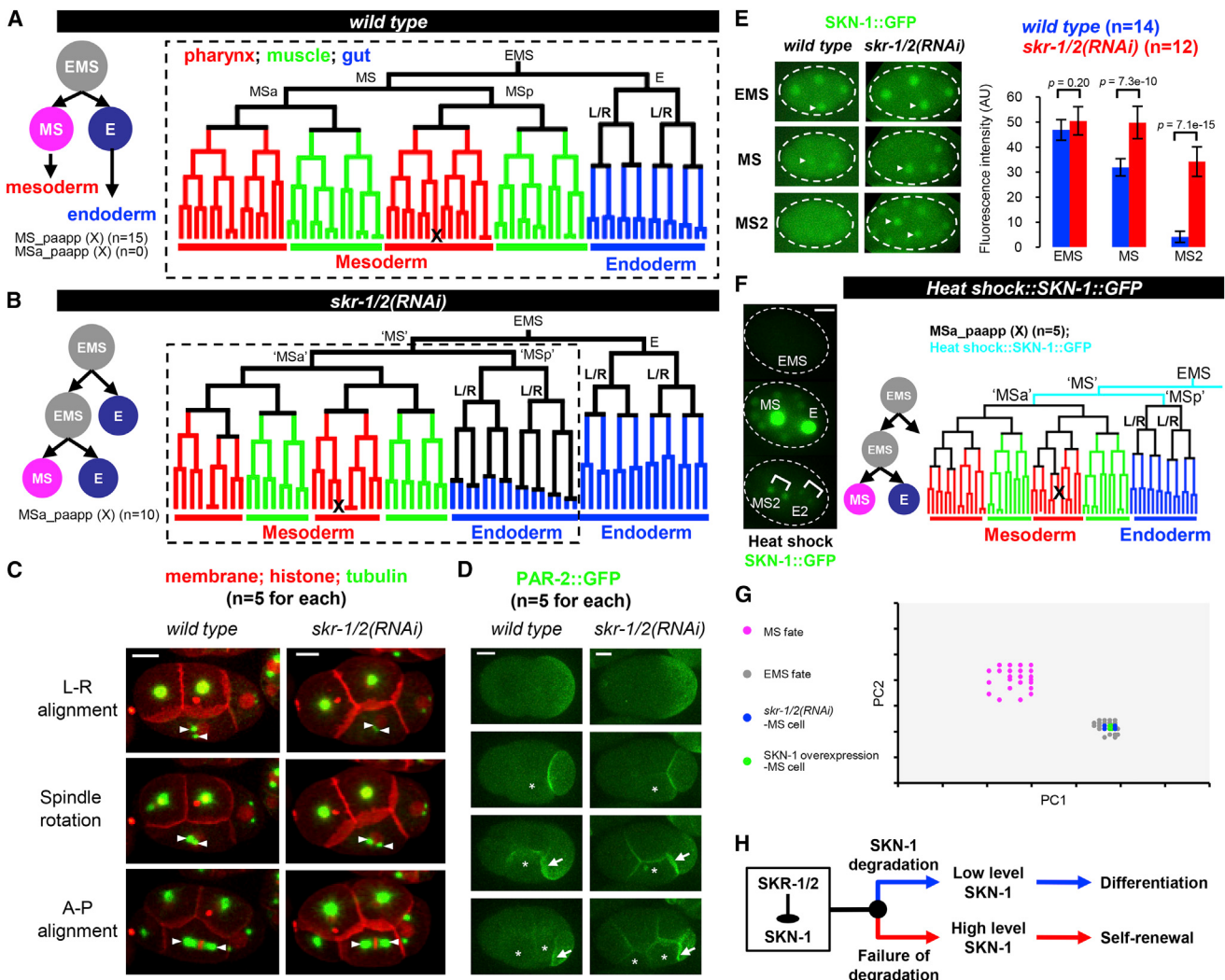


Figure 5. Protein Degradation Drives Transition of Cell Fate

(A) Transition of cell fate in the wild-type endomesodermal lineage. Colored tree shows expression of pharynx, muscle, and gut markers in EMS lineage. In addition to cell lineage and fate patterning, characteristic single-cell behaviors including cell death (X) and left-right cell division (L/R) are also shown. See also Figures S3A–S3D.

(B) MS acquires EMS fate in *skr-1/2(RNAi)*. See also Figures S3A–S3F.

(C and D) Fate of the EMS blastomere is specified correctly. (C) The ability of EMS to receive and respond to signals from the neighboring P₂ cell to rotate its spindle from an initial left-right alignment to anterior-posterior (Eisenmann, 2005). (D) The ability of EMS to signal to P₂ to orient PAR-2 polarity (Arata et al., 2010). Spindle (arrowheads) rotation in the EMS cell and PAR-2 polarity in P₂ (arrows) are indistinguishable between the wild-type and *skr-1/2(RNAi)*. Scale bar, 10 μm.

(E) *skr-1/2(RNAi)* causes delayed degradation of SKN-1. Left: micrographs of embryos with SKN-1::GFP expression (green). Arrowheads highlight EMS, MS and two MS daughter cells. SKN-1::GFP signal in other blastomeres at four-cell stage is due to the maternal load (Page et al., 2007). Right: quantification of SKN-1::GFP levels (mean ± SD; p value was estimated by two-tailed t test).

(F) Left: heat-shock-induced overexpression leads to sustained SKN-1::GFP in MS, E, and their daughter cells. Scale bar, 10 μm. Right: reiteration of EMS fate in MS under heat-shock-induced overexpression of SKN-1::GFP. See also Figure S3G.

(G) Quantitative analysis of cell fate. Scatterplot shows the distribution of CEPs of the MS cell in *skr-1/2(RNAi)* and SKN-1 overexpression relative to the normal MS and EMS fates in an abstract space.

(H) Summary of results.

signaling events for over 30-fold. It is worth noting that, as in any computational analyses, the predictions need further experimental validation, but the results suggest that our cell-cell network analysis provides a powerful approach to identify potential signaling events from complex phenotype data.

Integrated Model

We integrated the directed graph of fate progression, gene regulators, and cell-to-cell signaling into a mechanistic model of differentiation at a systems level (Figure 7). In the model, cell fates, trajectories of fate differentiation, and binary fate choices are

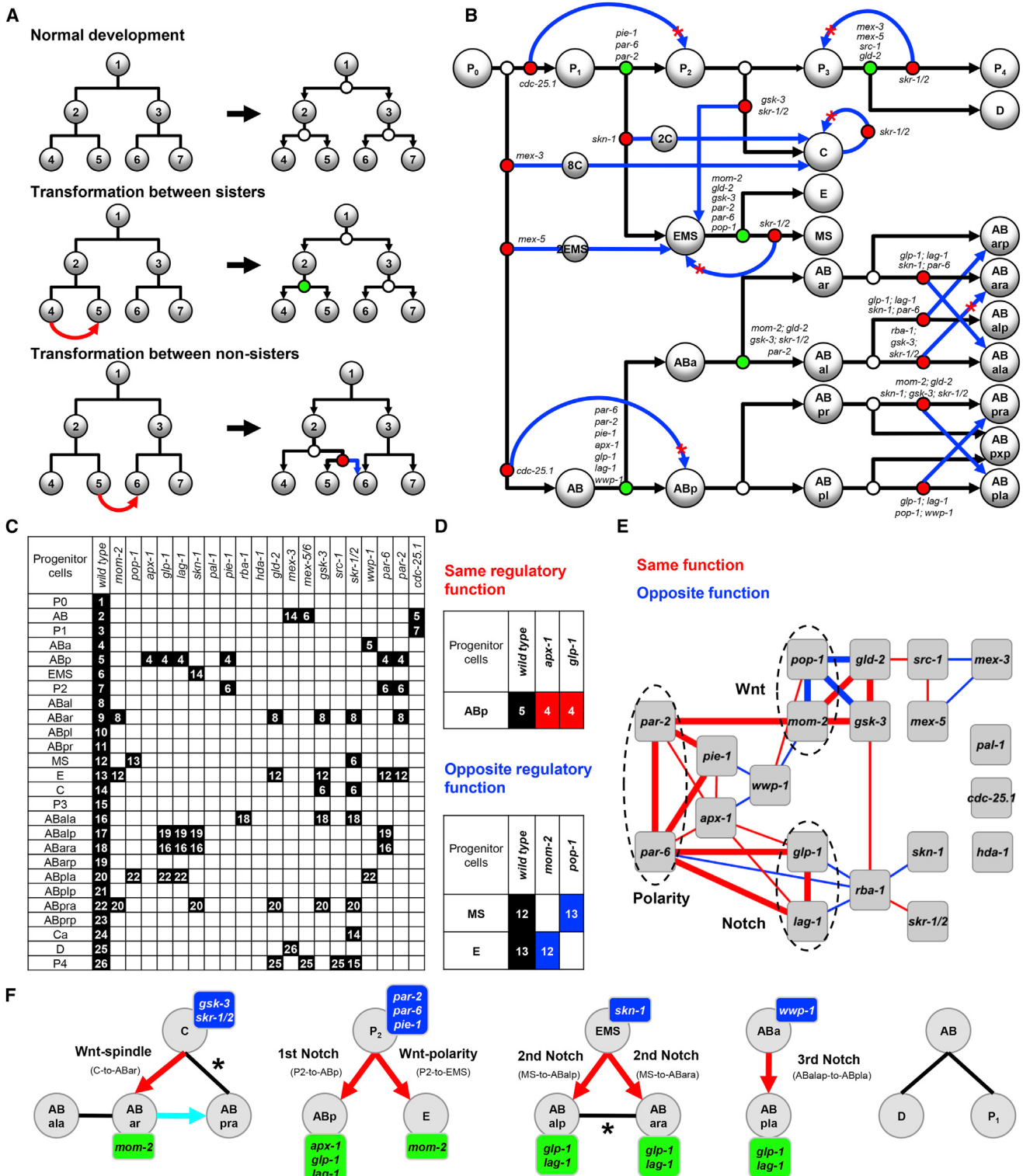


Figure 6. Systems-Level Analysis of Differentiation

(A) Rules to construct a directed graph of fate progression and fate choices. Top: wild-type cell lineage was used to construct a directed graph of fate (numbered nodes) progression (arrows) and binary fate choices (dots) during normal development. Middle and bottom: homeotic transformations (red arrows) were used to infer additional binary fate choices and trajectories of fate progression. See main text for details.

(legend continued on next page)

drawn as in Figure 6B. Genes are associated with the individual fate choices they regulate (Figure 7A, left). We defined the directionality of gene function arbitrarily. For homeotic transformation between sister fates, we drew the corresponding gene as a positive regulator of the fate it promotes. For transformations between nonsister fates, we drew the gene as a repressor of the alternative fate. If multiple genes regulate the same fate choice/bifurcation, the network topology is inherited from Figure 6E (Figure 7A, middle). This should not be confused with genetic epistasis among these genes, because our single-gene perturbations do not provide the required information to establish genetic epistasis. The exceptions are the Notch and Wnt pathway components, which are ordered based on their molecular identities.

The cell-cell network further reduces redundancy of information in the phenotype data set. When a gene affects two cells that are linked by a signaling event, we mapped the gene only to the signaling cell under the assumption that the gene functions indirectly in the receiving cell. Genes that affect only the receiving cell are considered components or modulators of the underlying signaling pathway (Figure 7A, right). Signaling events are drawn as thin yellow arrows originating from the predicted signaling cell and pointing to the presumed pathway components of the receiving cell.

Together, this molecular and cellular regulatory network summarizes how gene modules and signaling events regulate the progression of cell fate differentiation (Figure 7B). The information was extracted from 3D time-lapse images of development through a series of computational analyses (Figure 7C) and provides a systems-level view of the complex development processes of an early metazoan embryo with predicted *in vivo* regulatory mechanisms.

DISCUSSION

In summary, our study establishes an approach to automatically infer systems-level mechanistic models of development from live-imaging data. The CEP analysis and automated reasoning convert the large number of secondary phenotypes, namely the expression of tissue-specific markers in terminal cells, into the primary fate changes in the progenitor cells, which allows the additional inference of developmental mechanisms. Importantly, the cellular-resolution phenotype data enabled us to design novel systems biology analyses with rich biological

insights. The analyses allowed us to construct an explicit model of how cell fate differentiation progresses and to predict the gene-gene and cell-cell signaling networks during development. Additional discussion regarding the experimental design (choice of markers and alternative approaches of genetic perturbation) and computational design (robustness to experimental variations) is provided in the [Extended Experimental Procedures \(General Considerations\)](#) and Figure S4.

The automated reasoning and interpretation of phenotypes are based on general logic of developmental genetics without prior knowledge of gene function or the expectation of specific phenotypes. While the invariant cell lineage of *C. elegans* plays an important role in our study at the technical level, the logic used behind the automated reasoning as well as the approaches to implement the logic are designed to comply with regulative development and variable cell lineage. As shown in this study, the CEP analysis does not require an invariant cell lineage (Figures S1D–S1H) or an assumption of one cell per fate. However, it would require anatomy-based spatial registration of specimens so that equivalent cells can be identified and compared between samples. Automated spatial registration has been shown to be practical in complex organisms, especially with the aid of additional molecular markers (Fowlkes et al., 2008). Live imaging provides accessibility to many developmental processes *in vivo* in organisms with regulative development (Busch et al., 2012; Keller, 2013). Our study suggests that with continued cell-tracking improvements (Keller et al., 2010; Santella et al., 2010), automated approaches can also be successful in processing and interpreting the large amount of complex information in images to arrive at mechanistic insights in more complex organisms.

We envision that automated phenotype analyses like ours will greatly accelerate the study of development, where hundreds of mutants can be routinely analyzed with single-cell resolution to produce systems-level mechanistic models. Many animal groups exhibit invariable development as *C. elegans* but are understudied in terms of the genetic regulatory networks. Our approach allows *de novo* construction of mechanistic models of development without extensive prior knowledge. Hence, with genome sequencing, RNAi, and emerging tools for targeted genome engineering, as well as imaging-based cell lineage analysis, especially by differential interference contrast microscopy (Schnabel et al., 1997), the strategy described here can be applied to such organisms to rapidly broaden our understanding of the development of multicellular organisms.

(B) The graph integrating all results from the wild-type and the detected homeotic transformations. Nodes represent progenitor cell fates. Arrows represent trajectories of fate progression (black: trajectories inferred from normal development; blue: trajectories inferred from RNAi phenotypes; star: new trajectories revealed in this study). Points highlight binary fate choices (open: choice between sister fates inferred from normal development and not perturbed in our data set; green: choice between sister fates that were perturbed; red: choice between nonsister fates). The regulators are placed near the corresponding perturbed bifurcation points. When a fate can be transformed to more than one other fate, the corresponding trajectories and bifurcation points are ordered arbitrarily. Additional genetic experiments would be needed to order them. See also Figure S2C.

(C) Matrix summarizing all detected homeotic transformations. Fates of progenitor cells are indicated by numbers.

(D) Genes inducing identical transformations (e.g., 5 → 4) are considered as having same regulatory function and genes inducing opposite transformations (12 → 13 versus 13 → 12) are considered as having opposite function.

(E) Gene network. Edges with two or more shared phenotypes are shown in thick lines. Dashed circles highlight the three known genetic modules.

(F) Cell-cell network. Known events of Wnt and Notch signaling are highlighted by red arrows, from signaling cell to receiving cells. Genes in the corresponding signaling pathways that affect the receiving cell are labeled on the receiving cell (green boxes). Genes that perturb both cells are labeled on the signaling cell (blue). Cyan arrow represents an ectopic third Notch signal from ABar daughter (ABara) to ABra that occurs when ABar → ABal. Stars indicate redundant links that are inevitable in network inference.

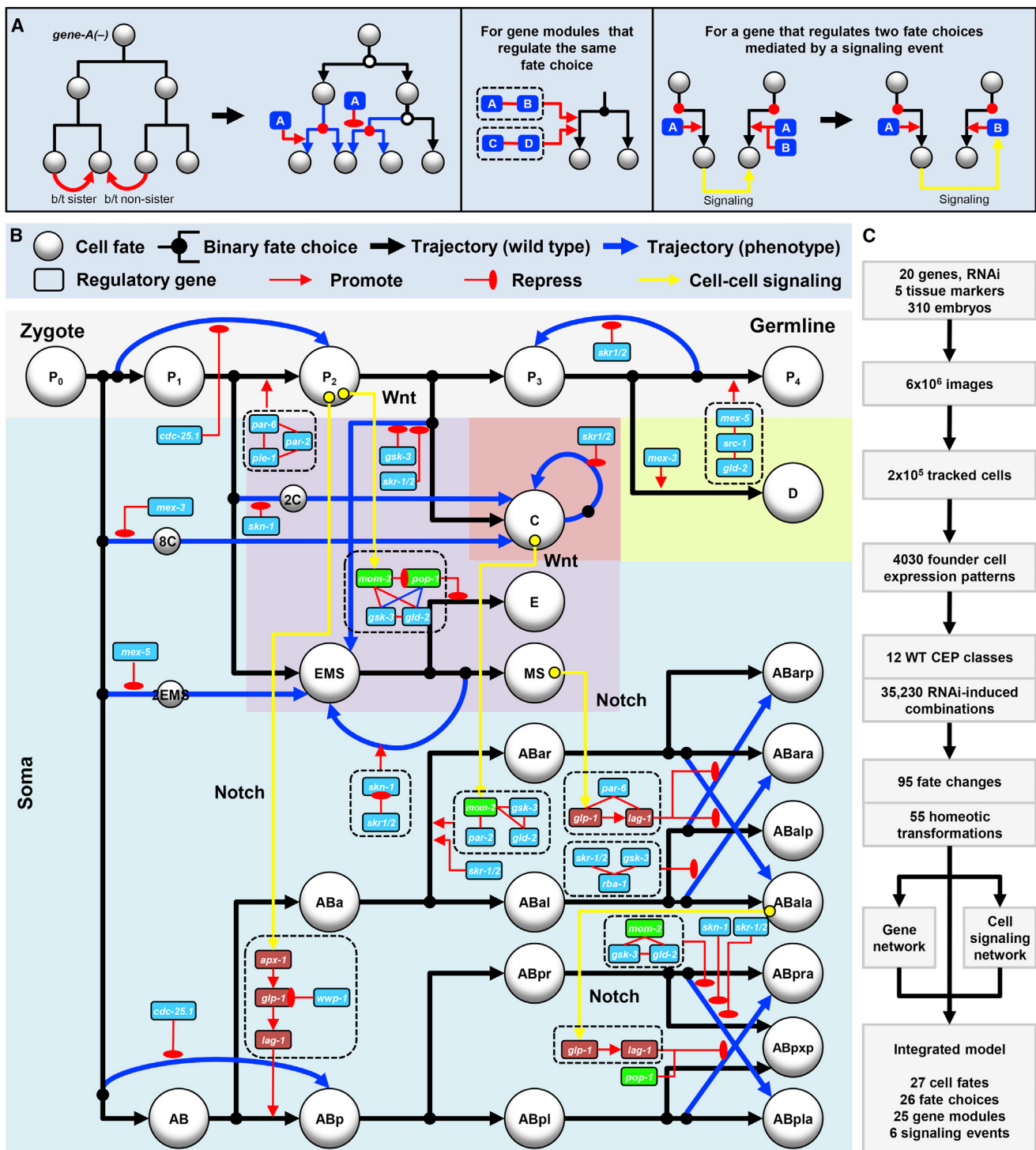


Figure 7. Inferred Mechanistic Model of Development

(A) Rules to integrate results. Left: a homeotic transformation phenotype is interpreted as a regulated binary fate choice, with the perturbed gene as the regulator at the corresponding bifurcation. Middle: genes with identical phenotype are organized based on topology of gene network (direct links) in Figure 6E to regulate fate choices. Right: cell-cell signaling is used to reduce redundant information of gene function. See main text for details.

(B) Integrated model based on this study. Fate progression and binary choices are represented as in Figure 6. Predicted Wnt and Notch signaling events are shown as yellow arrows from the signaling cell to the receiving cell. Genes in these pathways are colored as green (Wnt) and dark red (Notch) and ordered based on molecular identity.

(C) Flow of information.

EXPERIMENTAL PROCEDURES

All experimental procedures, including experimental and computational methods, are detailed in the [Extended Experimental Procedures](#).

SUPPLEMENTAL INFORMATION

Supplemental Information includes Extended Experimental Procedures, four figures, five tables, and one movie and can be found with this article online at <http://dx.doi.org/10.1016/j.cell.2013.11.046>.

ACKNOWLEDGMENTS

We thank J. Priess for critical discussions, J. Rothman, M. Maduro, J. Gaudet, J. Kimble, and B. Page for reagents; Q. Li and Y. Kamikawa for technical assistance; and I. Kovacevic and M. Pellegrino for critical reading of the manuscript. This work is partly supported by NIH grants (HD075602 and GM097576) to Z.B. Some strains were provided by the CGC, which is funded by NIH Office of Research Infrastructure Programs (P40 OD010440).

Received: June 4, 2013

Revised: September 25, 2013

Accepted: November 11, 2013

Published: January 16, 2014

REFERENCES

- Arata, Y., Lee, J.Y., Goldstein, B., and Sawa, H. (2010). Extracellular control of PAR protein localization during asymmetric cell division in the *C. elegans* embryo. *Development* **137**, 3337–3345.
- Bao, Z., Murray, J.I., Boyle, T., Ooi, S.L., Sandel, M.J., and Waterston, R.H. (2006). Automated cell lineage tracing in *Caenorhabditis elegans*. *Proc. Natl. Acad. Sci. USA* **103**, 2707–2712.
- Bao, Z., Zhao, Z., Boyle, T.J., Murray, J.I., and Waterston, R.H. (2008). Control of cell cycle timing during *C. elegans* embryogenesis. *Dev. Biol.* **318**, 65–72.
- Bowerman, B., Eaton, B.A., and Priess, J.R. (1992). *skn-1*, a maternally expressed gene required to specify the fate of ventral blastomeres in the early *C. elegans* embryo. *Cell* **68**, 1061–1075.
- Bowerman, B., Draper, B.W., Mello, C.C., and Priess, J.R. (1993). The maternal gene *skn-1* encodes a protein that is distributed unequally in early *C. elegans* embryos. *Cell* **74**, 443–452.
- Busch, W., Moore, B.T., Martsberger, B., Mace, D.L., Twigg, R.W., Jung, J., Pruteanu-Malinici, I., Kennedy, S.J., Fricke, G.K., Clark, R.L., et al. (2012). A microfluidic device and computational platform for high-throughput live imaging of gene expression. *Nat. Methods* **9**, 1101–1106.
- Eisenmann, D.M. (2005). Wnt signaling (June 25, 2005). *WormBook*, 1–17. <http://dx.doi.org/10.1895/wormbook.1.7.1>.
- Fowlkes, C.C., Hendriks, C.L., Keränen, S.V., Weber, G.H., Rübel, O., Huang, M.Y., Chatoor, S., DePace, A.H., Simirenko, L., Henriquez, C., et al. (2008). A quantitative spatiotemporal atlas of gene expression in the *Drosophila* blastoderm. *Cell* **133**, 364–374.
- Giurumescu, C.A., Kang, S., Planchon, T.A., Betzig, E., Bloomkatz, J., Yelon, D., Cosman, P., and Chisholm, A.D. (2012). Quantitative semi-automated analysis of morphogenesis with single-cell resolution in complex embryos. *Development* **139**, 4271–4279.
- Green, R.A., Kao, H.L., Audhya, A., Arur, S., Mayers, J.R., Fridolfsson, H.N., Schulman, M., Schloissnig, S., Niessen, S., Laband, K., et al. (2011). A high-resolution *C. elegans* essential gene network based on phenotypic profiling of a complex tissue. *Cell* **145**, 470–482.
- Gunsalus, K.C., Ge, H., Schetter, A.J., Goldberg, D.S., Han, J.D., Hao, T., Berriz, G.F., Bertin, N., Huang, J., Chuang, L.S., et al. (2005). Predictive models of molecular machines involved in *Caenorhabditis elegans* early embryogenesis. *Nature* **436**, 861–865.
- Hench, J., Henriksson, J., Lüppert, M., and Bürglin, T.R. (2009). Spatio-temporal reference model of *Caenorhabditis elegans* embryogenesis with cell contact maps. *Dev. Biol.* **333**, 1–13.
- Keller, P.J. (2013). Imaging morphogenesis: technological advances and biological insights. *Science* **340**, 1234168.
- Keller, P.J., Schmidt, A.D., Santella, A., Khairy, K., Bao, Z., Wittbrodt, J., and Stelzer, E.H. (2010). Fast, high-contrast imaging of animal development with scanned light sheet-based structured-illumination microscopy. *Nat. Methods* **7**, 637–642.
- Lehner, B., Crombie, C., Tischler, J., Fortunato, A., and Fraser, A.G. (2006). Systematic mapping of genetic interactions in *Caenorhabditis elegans* identifies common modifiers of diverse signaling pathways. *Nat. Genet.* **38**, 896–903.
- Liu, X., Long, F., Peng, H., Aerni, S.J., Jiang, M., Sánchez-Blanco, A., Murray, J.I., Preston, E., Mericle, B., Batzoglou, S., et al. (2009). Analysis of cell fate from single-cell gene expression profiles in *C. elegans*. *Cell* **139**, 623–633.
- Mace, D.L., Weisdepp, P., Govirtzman, L., Boyle, T., and Waterston, R.H. (2013). A high-fidelity cell lineage tracing method for obtaining systematic spatiotemporal gene expression patterns in *Caenorhabditis elegans*. *G3 (Bethesda)* **3**, 851–863.
- Megason, S.G., and Fraser, S.E. (2007). Imaging in systems biology. *Cell* **130**, 784–795.
- Moore, J.L., Du, Z., and Bao, Z. (2013). Systematic quantification of developmental phenotypes at single-cell resolution during embryogenesis. *Development* **140**, 3266–3274.
- Murray, J.I., Bao, Z., Boyle, T.J., Boeck, M.E., Mericle, B.L., Nicholas, T.J., Zhao, Z., Sandel, M.J., and Waterston, R.H. (2008). Automated analysis of embryonic gene expression with cellular resolution in *C. elegans*. *Nat. Methods* **5**, 703–709.
- Murray, J.I., Boyle, T.J., Preston, E., Vafeados, D., Mericle, B., Weisdepp, P., Zhao, Z., Bao, Z., Boeck, M., and Waterston, R.H. (2012). Multidimensional regulation of gene expression in the *C. elegans* embryo. *Genome Res.* **22**, 1282–1294.
- Page, B.D., Diede, S.J., Tenlen, J.R., and Ferguson, E.L. (2007). *EEL-1*, a Hect E3 ubiquitin ligase, controls asymmetry and persistence of the *SKN-1* transcription factor in the early *C. elegans* embryo. *Development* **134**, 2303–2314.
- Santella, A., Du, Z., Nowotschin, S., Hadjantonakis, A.K., and Bao, Z. (2010). A hybrid blob-slice model for accurate and efficient detection of fluorescence labeled nuclei in 3D. *BMC Bioinformatics* **11**, 580.
- Schnabel, R., and Priess, J.R. (1997). Specification of cell fates in the early embryo. In *C. elegans II*, Second Edition, D.L. Riddle, T. Blumenthal, B.J. Meyer, and J.R. Priess, eds. (Cold Spring Harbor, NY: Cold Spring Harbor Laboratory Press), pp. 361–382.
- Schnabel, R., Hutter, H., Moerman, D., and Schnabel, H. (1997). Assessing normal embryogenesis in *Caenorhabditis elegans* using a 4D microscope: variability of development and regional specification. *Dev. Biol.* **184**, 234–265.
- Sönnichsen, B., Koski, L.B., Walsh, A., Marschall, P., Neumann, B., Brehm, M., Alleaume, A.M., Artelt, J., Bettencourt, P., Cassin, E., et al. (2005). Full-genome RNAi profiling of early embryogenesis in *Caenorhabditis elegans*. *Nature* **434**, 462–469.
- Sulston, J.E., Schierenberg, E., White, J.G., and Thomson, J.N. (1983). The embryonic cell lineage of the nematode *Caenorhabditis elegans*. *Dev. Biol.* **100**, 64–119.